SAND80-0475
Unlimited Release
UC-60

Torque Ripple in a Darrieus, Vertical Axis Wind Turbine

Robert C. Reuter, Jr

Prepared by Sandia Laboratories, Albuquerque, New Mexico 87185
and Livermore, California 94550 for the United States Department
of Energy under Contract DE-AC04-76DP00789

September 1980

Sandia National Laboratories

SF 2900-Q(3-80)

Issued by Sandia Laboratories, operated for the United States Department of Energy by Sandia Corporation.

NOTICE

This report was prepared as an account of work sponsored by the United States Government. Neither the United States nor the Department of Energy, nor any of their employees, nor any of their contractors, subcontractors, or their employees, makes any warranty, express or implied, or assumes any legal liability or responsibility for the accuracy, completeness or usefulness of any information, apparatus, product or process disclosed, or represents that its use would not infringe privately owned rights.

SF 1004-DF(11-77)

Printed in the United States of America
Available from:
National Technical Information Service
U. S. Department of Commerce
5285 Port Royal Road
Springfield, VA 22161

NTIS Price Codes

Printed Copy $6.00; Microfiche: A01

SAND80-0475
Unlimited Release
Printed September 1980

TORQUE RIPPLE IN A DARRIEUS, VERTICAL AXIS WIND TURBINE

Robert C. Reuter, Jr.
Applied Mechanics Division III, 5523
Sandia National Laboratories
Albuquerque, New Mexico 87185

ABSTRACT

Interaction between a steady wind and a rotating, Darrieus, vertical axis wind turbine produces time periodic aerodynamic loads which cause time dependent torque variations, referred to as torque ripple, to occur in the mechanical link between the turbine and the electrical generator. There is concern for the effect of torque ripple upon fatigue life of drive train components and upon power quality. An analytical solution characterizing the phenomenon of torque ripple has been obtained which is based upon a Fourier expansion of the time dependent features of the problem. Numerical results for torque ripple, some experimental data, determinatioin of acceptable levels and methods of controlling it, are presented and discussed.

INTRODUCTION

In a utility grid application, power gathered from the wind by a Darrieus, vertical axis wind turbine (VAWT), Fig. 1, operating synchronously, is in the form of mechanical torque at a specified rotational speed. Interaction of the rotating blades with the incident wind causes a time periodicity in the net torque acting on the turbine, which is obtained by integrating torque producing aerodynamic loads over all blades present. Under the ideal conditions of a steady wind from a fixed direction, the applied torque may be viewed as a deterministic oscillation called torque ripple, (which may contain many harmonics) superimposed on a steady, mean torque, which is relatable to overall turbine performance. Depending upon turbine operating conditions (such as wind speed and turbine RPM) and upon drive train characteristics (such as component inertia properties and torsional rigidities, gear ratios and generator slip) the magnitude of the oscillations may be either amplified or attenuated at various locations along the drive train. In view of extended component fatigue life and high power quality requirements, attenuation of torque ripple to acceptable levels is highly desirable.

Recognition of the torque ripple problem and its consequences, and attempts to characterize it analytically and demonstrate control over it are not new[1,2]. Two of the assumptions upon which early analytical work on torque ripple in VAWT systems was based[1] are as follows: 1. The wind is steady and from a fixed direction, and 2. The net torque applied to the turbine is a simple harmonic function of time. Models based on these assumptions captured torque ripple behavior trends as parameters were changed[1] and permitted at least initial insights toward understanding the problem.

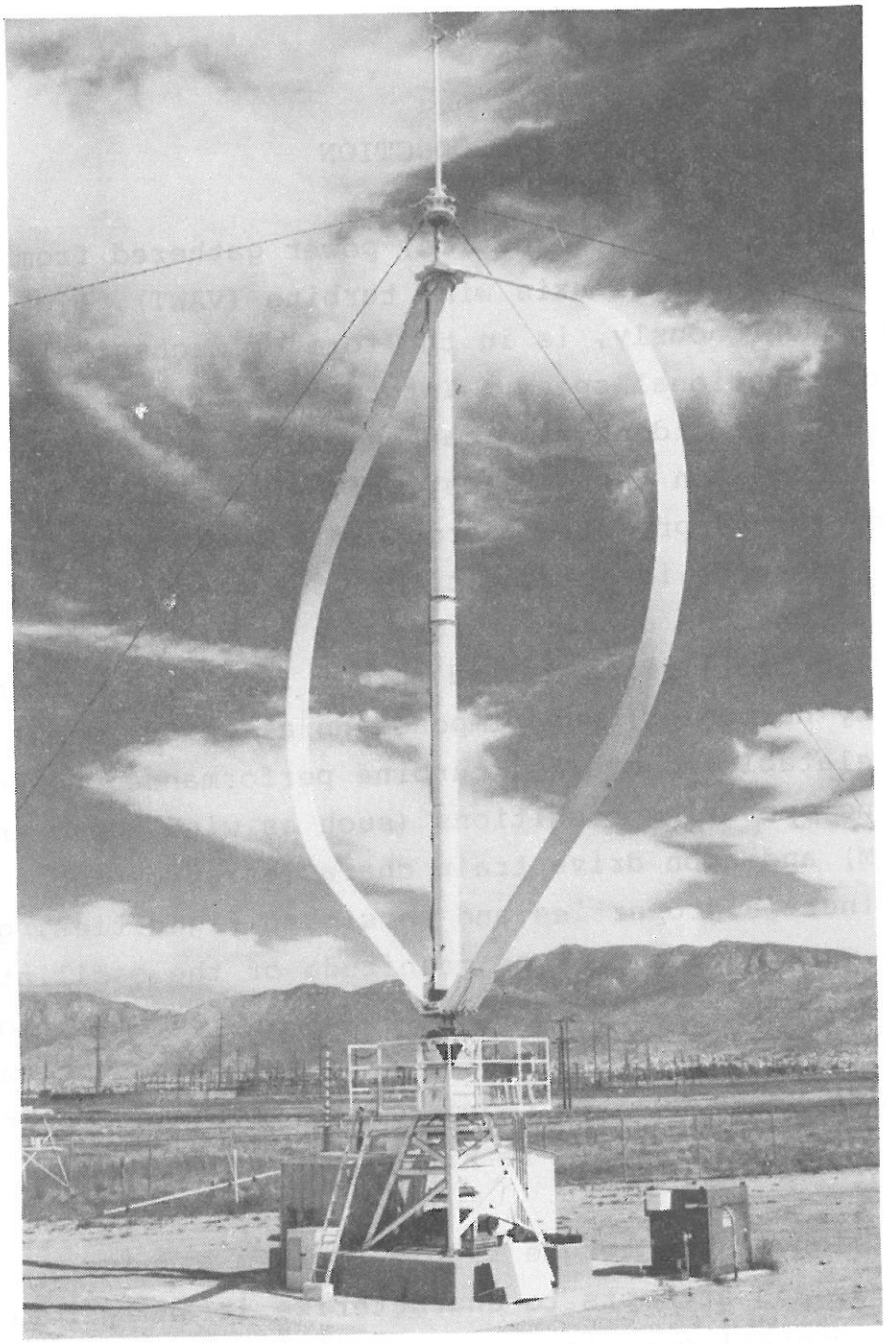

Figure 1. DOE/Sandia 17-meter, 60 KW, Darrieus, vertical axis wind turbine located in Albuquerque, New Mexico.

However, recent aerodynamic models[3], from which come the magnitude and time dependence of the net aerodynamic torque applied to the turbine, demonstrate that the assumption of a simple harmonic form for the applied torque is not always

justified. Asymmetries in the upwind and downwind aerodynamics[3], and the temporal influence of stall at high wind speeds, (a previously known result)[4], cause multiple harmonics to appear in the applied torque, even for a fixed wind. By using a Fourier expansion of the time dependent characteristics of the torque ripple problem, a general solution has been obtained which permits full representation of the consequences of upwind and downwind aerodynamnic asymmetries and blade stall. This approach, along with numerical results, a limited amount of data correlation, and a discussion of how acceptable torque ripple levels are determined and achieved, is presented. With appropriate modifications, this analysis may be used to study torque ripple in horizontal axis and other vertical axis wind energy systems.

THE TORQUE RIPPLE MODEL

A typical VAWT drive train consists of the turbine rotor (blades and rotating tower), a transmission and a generator, connected in series by various torque transmitting shafts and couplings. Additional components may be present depending upon the specific turbine design, purpose and installation. For example, the DOE/Sandia 17-meter research turbine[5] located in Albuquerque, NM, Fig. 1, has a secondary gear ratio change capability in the form of interchangeable pulleys and a timing belt, located between the transmission (which has a fixed gear ratio) and the generator. This feature permits incremental changes in the turbine operating speed and allows field evaluation of aerodynamic, structural and system performance, in a synchronous mode, under a variety of operating conditions. "Operating conditions" refers collectively to combinations of incident wind velocity and turbine operating speed. A popular parameter characterizing operating conditions

is tip speed ratio, λ, which is equal to maximum blade speed, $R_{MAX}\Omega$, divided by incident wind speed, V. When $\lambda \geq 3.5$ the simple harmonic representation of applied torque and drive train response is justified[1,3,4], as seen in Fig. 2.

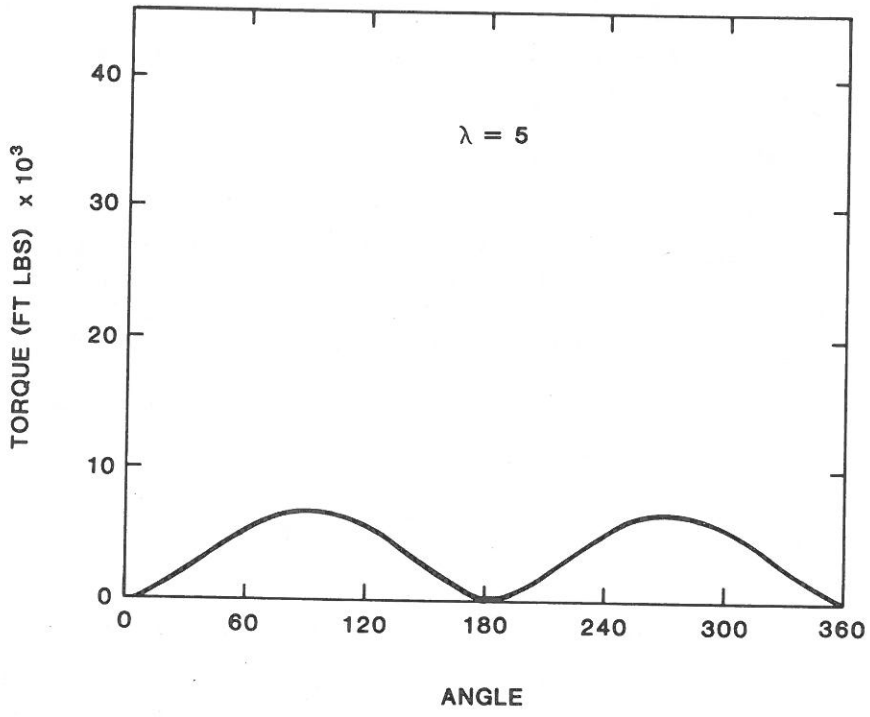

Figure 2. Applied torque versus azimuth position for one turbine revolution when $\lambda = 5.0$

However, when $\lambda \leq 3.5$, blade stall effects and upwind and downwind aerodynamic asymmetries become strong[3,4], thus compelling a Fourier expansion of torque ripple time characteristics, see Fig. 3. Since peak turbine power and, therefore, peak mean torque occurs at a tip speed ratio in the range of 1.0 to 3.0,[5], it is essential that dynamic behavior of the turbine be well understood for low values of λ.

The torque ripple model consists of three essential elements. The first is a simplified, physical representation of the important characteristics of the entire drive train for

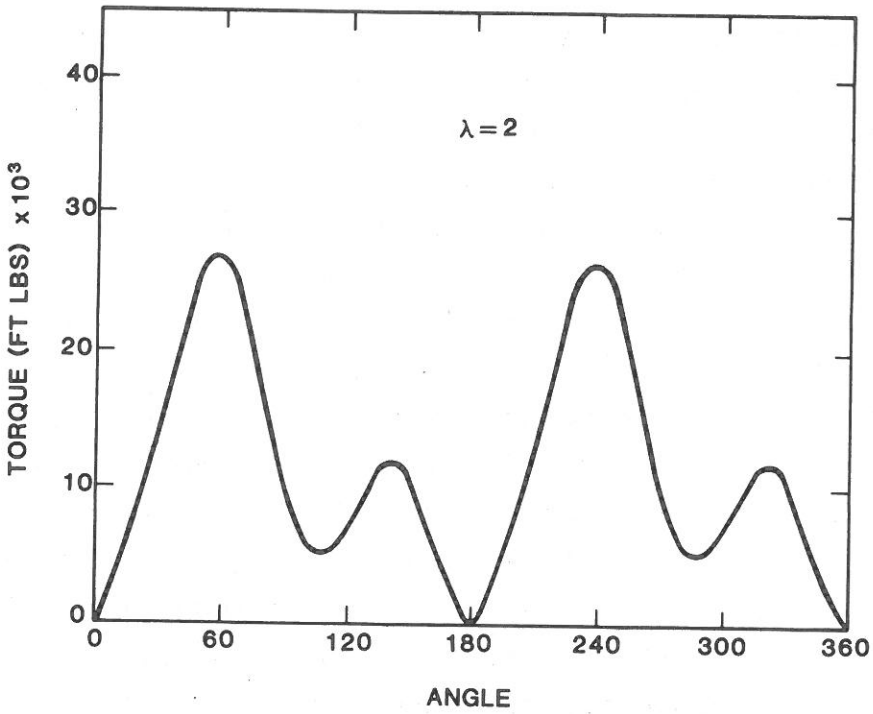

Figure 3. Applied torque versus azimuth position for one turbine revolution when $\lambda = 2.0$

which differential equations of motion can be written. Fig. 4 shows the physical model chosen. The turbine rotor is represented by two rotational inertias, the positions of which are specified by θ_1 and θ_2, each with one-half of the total

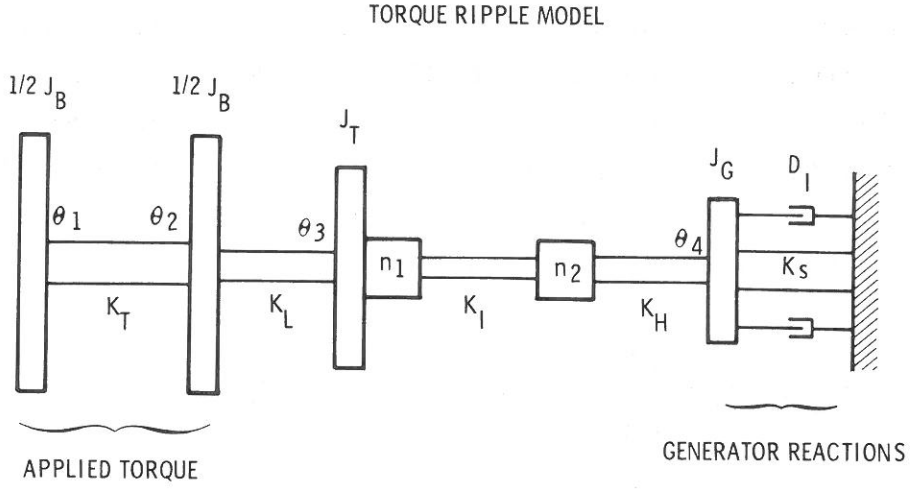

Figure 4. Schematic of turbine drive train components and nomenclature.

rotor inertia, and which are connected together by a torsional shaft representing the rotor tower, with a stiffness, K_T, chosen to yield the correct counter-rotating frequency for the rotor. Continuing downstream, the equivalent low speed shaft (stiffness = K_L) transmits torque to the transmission with its inertia, J_T, fixed gear ratio, n_1, and position, θ_3. The interchangeable pulleys and timing belt have an incrementally adjustable, but operationally fixed gear ratio, n_2, and are connected upstream to the transmission with an equivalent intermediate speed shaft (stiffness = K_I) and downstream to an electric generator with an equivalent high speed shaft (stiffness = K_H). The electric generator (inertia = J_G and position = θ_4) may be either synchronous or induction, with torque reactions proportional to rotational position or speed, respectively. The proportionality constant is K_S for a synchronous generator, and D_I for an induction generator. Although results in this work are limited to those for an induction generator only, K_S is retained in the solution for generality. This physical representation of the drive train captures torsional vibration modes of interest.

The second element of the torque ripple model embodies a decomposition[6] of the functional dependence upon time of the applied aerodynamic torque as predicted by the vortex model[3] for low tip speed ratios and the stream tube models[4] for high tip speed ratios. (Changing from the vortex to the stream tube models is done to conserve computer time and reduce computation cost). The applied torque can be distributed fractionally between the two rotor inertias in order to account for vertical wind shear, if necessary, and has the form

$$T_{1A} = T_{10} + \sum_{i=1}^{N} T_{1i} \cos \omega_i t + \sum_{i=1}^{N} \overline{T}_{1i} \sin \omega_i t$$

$$T_{2A} = T_{20} + \sum_{i=1}^{N} T_{2i} \cos \omega_i t + \sum_{i=1}^{N} \overline{T}_{2i} \sin \omega_i t \qquad (1)$$

T_{1A} and T_{2A} are applied to the top (upstream) half and bottom (downstream) half of the rotor, respectively.

The third model element consists of a solution to the equations of motion, taken in the form

$$\theta_j = A_{j0} + \sum_{i=1}^{N} A_{ji} \cos \omega_i t + \sum_{i=1}^{N} \bar{A}_{ji} \sin \omega_i t + \Omega_j t \qquad (2)$$

where, repeating, θ_1 and θ_2 are the angular positions of the top and bottom rotor halves, respectively, θ_3 is the angular position of the low speed end of the transmission and θ_4 is the angular position of the generator. $\Omega_1 (= \Omega_2)$ is the mean operating speed of the turbine, Ω_3 is the mean speed of the slow speed end of the transmission, and Ω_4 is the mean operating speed of the generator (note that $\Omega_3 = \Omega_4/n_1n_2$). Since torsional modes of the turbine system which are reacted by torque in the drive train are even multiples of the operating speed[7], $\omega_i = 2i\Omega_1$.

Equations of motion for the physical representation of the torque ripple model depicted by Fig. 4 are

$$\begin{aligned}
&\tfrac{1}{2} J_B \ddot{\theta}_1 + K_T(\theta_1 - \theta_2) = T_{1A} \\
&\tfrac{1}{2} J_B \ddot{\theta}_2 + K_L(\theta_2 - \theta_3) + K_T(\theta_2 - \theta_1) = T_{2A} \\
&J_T \ddot{\theta}_3 + K_3\left(\theta_3 - \frac{\theta_4}{n_1 n_2}\right) + K_L(\theta_3 - \theta_2) = 0 \\
&J_G \ddot{\theta}_4 + K_4(\theta_4 - n_1 n_2 \theta_3) + K_S(\theta_4 - \omega_S t) + D_I(\dot{\theta}_4 - \omega_S) = 0
\end{aligned} \qquad (3)$$

After a substitution of (1) and (2) into (3), and a substantial amount of algebra, the following results are obtained for determination of the unknown constants.

$$A_{1i} = \frac{\lambda_{2i}\lambda_{3i} - \lambda_{1i}\lambda_{4i}}{(\lambda_{1i}^2 + \lambda_{2i}^2)} \quad , \quad \bar{A}_{1i} = \frac{\lambda_{1i}\lambda_{3i} + \lambda_{2i}\lambda_{4i}}{(\lambda_{1i}^2 + \lambda_{2i}^2)}$$

$$A_{2i} = \frac{\phi_{1i}A_{1i} - T_{1i}}{K_T} \quad , \quad \bar{A}_{2i} = \frac{\phi_{1i}\bar{A}_{1i} - \bar{T}_{1i}}{K_T}$$

$$A_{3i} = \frac{1}{K_T K_L}\left[\left(\phi_{1i}\phi_{2i} - K_T^2\right) A_{1i} - \left(K_T T_{2i} + \phi_{2i} T_{1i}\right)\right]$$

$$\bar{A}_{3i} = \frac{1}{K_T K_L}\left[\left(\phi_{1i}\phi_{2i} - K_T^2\right) \bar{A}_{1i} - \left(K_T \bar{T}_{2i} + \phi_{2i} \bar{T}_{1i}\right)\right]$$

$$A_{4i} = \frac{n_1 n_2}{K_T K_L K_3}\left\{\left[\phi_{3i}\left(\phi_{1i}\phi_{2i} - K_T^2\right) - \phi_{1i}K_L^2\right] A_{1i} + \left[K_L^2 T_{1i} - \phi_{3i}\left(K_T T_{2i} + \phi_{2i} T_{1i}\right)\right]\right\}$$

$$\bar{A}_{4i} = \frac{n_1 n_2}{K_T K_L K_3}\left\{\left[\phi_{3i}\left(\phi_{1i}\phi_{2i} - K_T^2\right) - \phi_{1i}K_L^2\right] \bar{A}_{1i} + \left[K_L^2 \bar{T}_{1i} - \phi_{3i}\left(K_T \bar{T}_{2i} + \phi_{2i} \bar{T}_{1i}\right)\right]\right\}$$

where

$$\phi_{1i} = \left(K_T - \omega_i^2 J_B/2\right) \quad , \quad \phi_{2i} = \left(K_T + K_L - \omega_i^2 J_B/2\right)$$

$$\phi_{3i} = \left(K_L + K_3 - \omega_i^2 J_T\right) \quad , \quad \phi_{4i} = \left(K_4 + K_S - \omega_i^2 J_G\right)$$

$$\lambda_{1i} = \omega_i D_I \left[\phi_{3i}\left(\phi_{1i}\phi_{2i} - K_T^2\right) - \phi_{1i} K_L^2\right]$$

$$\lambda_{2i} = \left(\phi_{3i}\phi_{4i} - K_3 K_4\right)\left(\phi_{1i}\phi_{2i} - K_T^2\right) - \phi_{1i}\phi_{4i} K_L^2$$

$$\lambda_{3i} = \left(\phi_{3i}\phi_{4i} - K_3K_4\right)\left(K_T T_{2i} + \phi_{2i} T_{1i}\right) - \phi_{4i} K_L^{\,2} T_{1i}$$

$$- \omega_i D_I \left[K_L^{\,2} \overline{T}_{1i} - \phi_{3i}\left(K_T \overline{T}_{2i} + \phi_{2i}\, \overline{T}_{1i}\right)\right]$$

$$\lambda_{4i} = \left(\phi_{3i}\phi_{4i} - K_3K_4\right)\left(K_T \overline{T}_{2i} + \phi_{2i} \overline{T}_{1i}\right) - \phi_{4i} K_L^{\,2} \overline{T}_{1i}$$

$$+ \omega_i D_I \left[K_L^{\,2} T_{1i} - \phi_{3i}\left(K_T T_{2i} + \phi_{2i} T_{1i}\right)\right]$$

$$K_3 = \frac{n_1^{\,2} n_2^{\,2} K_I K_H}{K_I + n_2^{\,2} K_H}$$

$$K_4 = K_3 / n_1^{\,2} n_2^{\,2}$$

which completes the solution derivation.

NUMERICAL RESULTS AND ALLOWABLE LEVELS

Numerical results presented here are based on drive train properties of the present DOE/Sandia 17-meter research turbine. They are:

$J_B = 2.92 \times 10^5$ lb-sec^2-in (3.30×10^4 N-sec^2-m)

$J_T = 2.15 \times 10^3$ lb-sec^2-in (2.43×10^2 N-sec^2-m)

$J_M = 27.1$ lb-sec^2-in (3.06 N-sec^2-m)

$D_I = 824.0$ lb-in-sec/rad (93.1 N-m-sec/rad)

$K_T = 1.46 \times 10^8$ lb-in/rad (1.65×10^6 N-m/rad)

$K_L = 2.39 \times 10^6$ lb-in/rad (2.69×10^5 N-m/rad)

$K_I = 1.25 \times 10^6$ lb-in/rad (1.41×10^5 N-m/rad)

$K_H = 1.86 \times 10^4$ lb-in/rad (2.10×10^3 N-m/rad)

$n_1 = 35.6$

$$n_2 = \frac{1800}{n_1(\Omega)}$$

$T_R = 8.35 \times 10^3$ ft-lb (1.13×10^2 N-m)

where 1800 is the rotational speed of the generator and Ω is the rotational speed of the turbine, both in units of RPM, and T_R is the torque rating of the turbine. Before defining torque ripple explicitly, it is necessary to derive an expression for torque as a function of time for some specified drive train location. After preliminary numerical evaluation, it was observed that, for the above set of properties, torque ripple in the drive train is essentially independent of location. Therefore, it is only necessary to know the torque in the low speed end, $T_L(t)$. It is given by $T_L(t) = K_L(\theta_3 - \theta_2)$, and with the above solution

$$T_L(t) = K_2 \left[\sum_{i=1}^{N} \left(A_{3i} \cos \omega_i t + \bar{A}_{3i} \sin \omega_i t \right) - \sum_{i=1}^{N} \left(A_{2i} \cos \omega_i t + \bar{A}_{2i} \sin \omega_i t \right) - \frac{T_{10} + T_{20}}{K_L} \right] \tag{4}$$

Torque ripple is defined in two ways. The first, labeled $\tilde{T}_M$, is the ratio of the mean-to-peak value and the mean value of torque, and is a convenient form when considering fatigue characteristics of the drive train components. The second, labled $\tilde{T}_R$, is the ratio of the mean-to-peak value and the turbine's rated torque, and is relatable to power quality. Thus, from (4)

$$\tilde{T}_M = \frac{T_{LMAX} - T_{LMIN}}{T_{LMAX} + T_{LMIN}} \tag{5}$$

$$\tilde{T}_R = \frac{T_{LMAX} - T_{LMIN}}{2\, T_{LRATED}} \tag{6}$$

In order to facilitate numerical evaluation of torque ripple a computer code, named FATE, was written. Applied torque coefficients, found in (1), are used as input to the code and results for $\tilde{T}_M$ and $\tilde{T}_R$ are calculated for discrete values of λ. (The coefficients of (1) vary with λ). Fig. 5 shows how torque ripple, using both definitions, varies with tip speed ratio for the DOE/Sandia research turbine operating at 50.6 rpm.

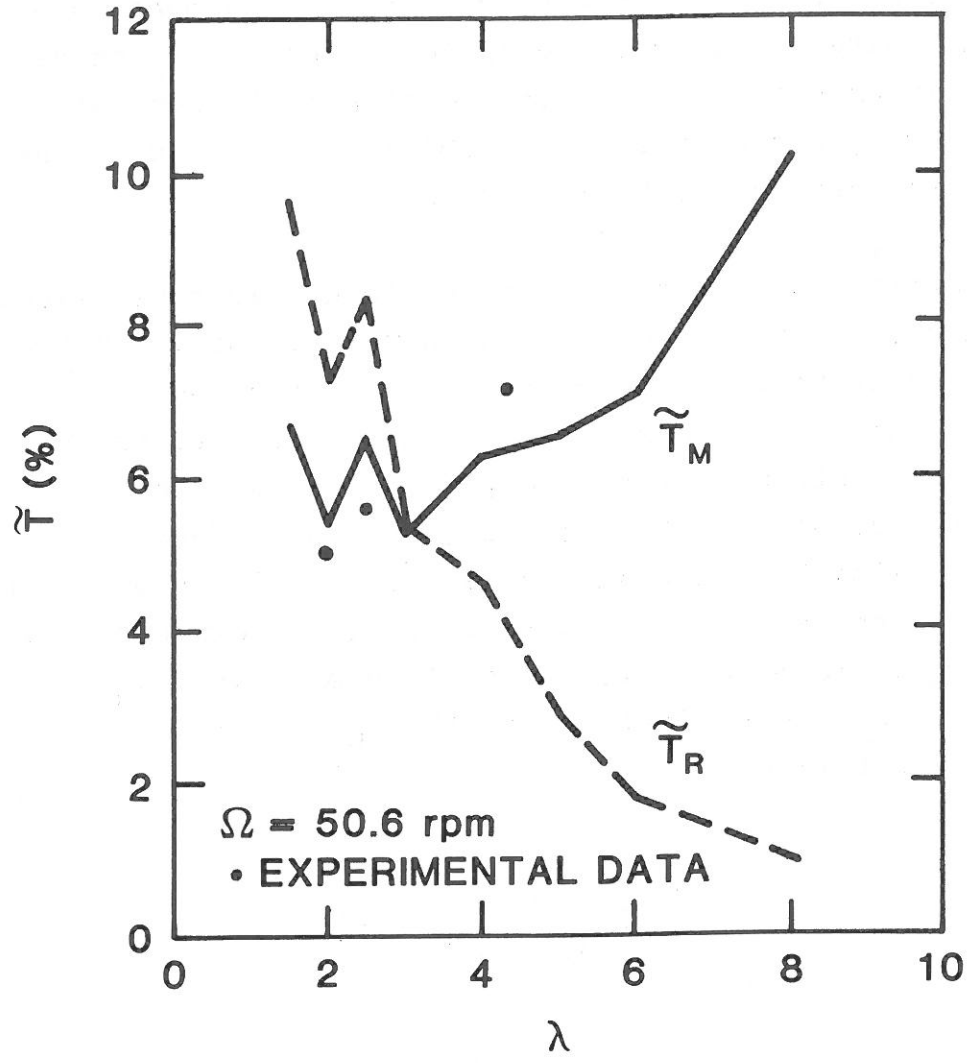

Figure 5. Torque ripple versus tip speed ratio for the DOE/Sandia research turbine operating at 50.6 RPM.

Because of the rapid changes in $\tilde{T}$ at low values of λ, calculated points are connected by straight lines. Three data points, based on the $\tilde{T}_M$ definition, are shown in the figure and agree closely with predicted values of $\tilde{T}_M$. These data are obtained by a torque sensor located in the low speed end of the drive train. More data are not presented because of the difficulty in obtaining experimental information not influenced by the random nature of the wind. Notice that $\tilde{T}_M$ increases with λ. This occurs because even though the oscillating portion of the torque is diminishing with λ, the mean value is diminishing faster, thus causing $\tilde{T}_M$ to increase. $\tilde{T}_R$ shows the change in only the oscillating portion of torque (since it is normalized by a constant--the turbine rated torque), where it is seen to decrease with increasing λ.

To determine what level of torque ripple might be allowable from a fatigue or life expectancy standpoint, assume that drive train components follow the Goodman law for fatigue strength[8]. This law imposes a straight line relationship between fatigue strength for purely alternating stress (the dependent variable) and mean stress (the independent variable). Using this law and the above definition of torque ripple expressed as a % of mean torque, $\tilde{T}_M$, an expression for allowable $\tilde{T}_M$ in terms of expected fatigue strength, σ_N, mean stress, σ_M, and ultimate strength, σ_U, of drive train components was derived. It is

$$\tilde{T}_M \leq \left(\frac{\sigma_N}{\sigma_U}\right)\left(\frac{\sigma_U}{\sigma_M} - 1\right) \qquad (7)$$

Taking the fatigue limit for σ_N, a typical value of the ratio, (σ_N/σ_U), for structural steels is 0.4. Using this value,

(7) can be plotted versus the ratio (σ_U/σ_M) as in Fig. 6. Since (σ_U/σ_M) may be viewed as a safety factor for design of drive train components, whatever value is used can be located on the ordinate of Fig. 6, and as long as the $\tilde{T}_M$ calculated from (5), falls on or below the line in Fig. 6, infinite life can be expected. By taking the ratio, $\tilde{T}_R/\tilde{T}_M$,

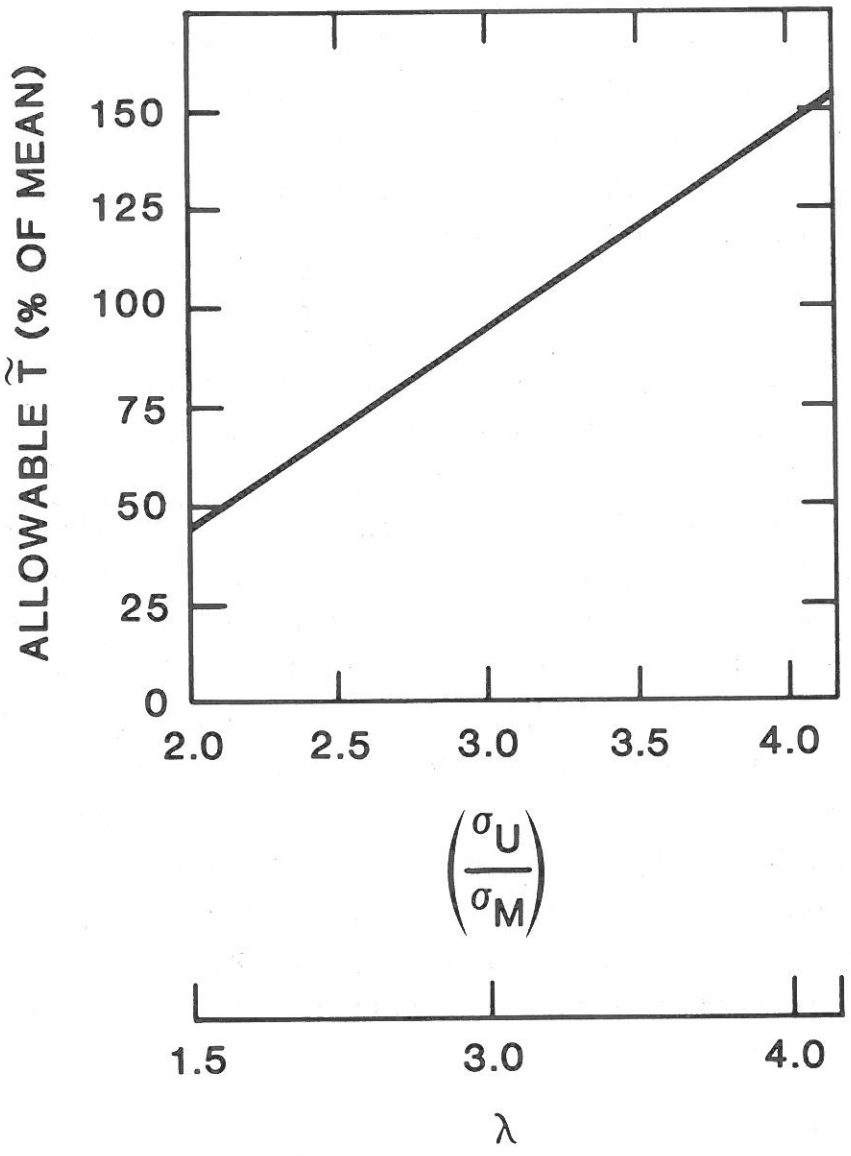

Figure 6. Allowable values of torque ripple (expressed as a % of mean torque) based on infinite life of drive train components.

for specific values of λ (for example from Fig. 5), it can be seen that as λ increases, σ_M decreases. Thus, increasing λ corresponds to an increase in (σ_U/σ_M) and, therefore, an increase in acceptable levels of $\tilde{T}_M$. For the DOE/Sandia research turbine, a design safety factor of 2.0 was used for drive train components. Since maximum torque occurs at $\lambda \simeq 1.5$, $(\sigma_U/\sigma_M) = 2.0$ on the abscissa in Fig. 6 corresponds to $\lambda = 1.5$. Using Fig. 5, it can be seen that $(\sigma_U/\sigma_M) \simeq 3.0$ corresponds to $\lambda = 3.0$, $(\sigma_U/\sigma_M) \simeq 4$ corresponds to $\lambda = 4.0$, and $(\sigma_U/\sigma_M) \simeq 6.5$ corresponds to $\lambda = 6$. This demonstrates that the allowable values of $\tilde{T}_M$ increase rapidly with λ. Examination of the values of $\tilde{T}_M$ in Fig. 5 indicates that the DOE/Sandia research turbine does not have a fatigue problem.

Power companies have determined that power quality determination is dominated by the amount of "light flicker" that people will tolerate for extended periods of time[9]. They have also determined that the "borderline of irritation" with 60 cycle power corresponds to a voltage variation of 0.5% of the line voltage. (This percent variation may be higher if energy is used only to power electrical equipment.) Since torque ripple in a generator is equivalent to current ripple in the line, acceptable torque ripple (expressed as a % of rated torque) can be related to voltage ripple. In the case of the DOE/Sandia research turbine, line impedance is approximately 4% of the load impedance. A maximum voltage ripple of 0.5%, therefore, corresponds to an allowable $\tilde{T}_R$ of 12.5%. Results in Fig. 5 indicate that the research turbine does not have a power quality problem.

CONTROL OF TORQUE RIPPLE

Among the properties which characterize the torque ripple problem, the most readily and easily modified are drive train

torsional rigidities and perhaps, generator slip. Fig. 7 shows numerical results for $\tilde{T}_M$ versus λ for the research turbine

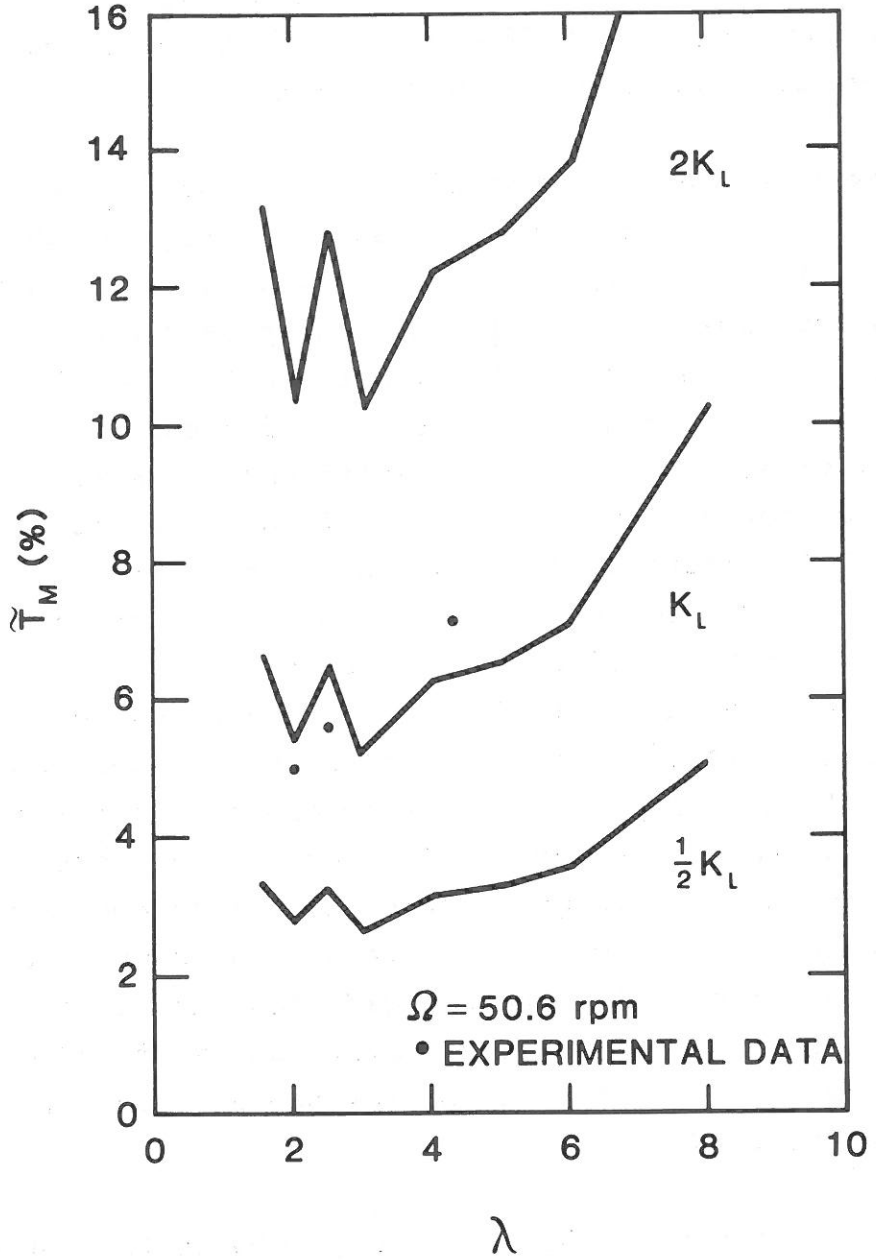

Figure 7. Torque ripple (expressed as a % of mean torque) versus tip speed ratio for various values of low speed drive train stiffness.

and values which would have resulted from a doubling and a halving of the torsional rigidity of the low speed end of its drive train. While fatigue life does not appear to be reduced even with a doubling of the low speed stiffness, additional rigidity increases could cause problems. Since $\tilde{T}_R \simeq \tilde{T}_M$ when $\lambda \simeq 1.5$, doubling the stiffness of the low speed end could cause a noticeable reduction in power quality.

To see how a change in low speed torsional stiffness effects torque ripple, consider the results in Fig. 8, where $\tilde{T}_M$ is plotted, for three low speed rigidities, as a function of turbine operating speed, Ω. Notice how the peak (which corresponds to the first critical drive train frequency) moves to the left with a reduction in low speed stiffness and to the right for an increase in drive train stiffness. The effect that this has on torque ripple at a specified operating speed is obvious. (This figure does not depict what occurs during start up. It provides torque ripple values in the drive train at specified operating speeds.) The behavior of $\tilde{T}_R$ with Ω is similar to that shown for $\tilde{T}_M$ in Fig. 8. Other methods of controlling torque ripple exist. An increase in generator slip tends to lower torque ripple values at moderate Ω, and increase them at higher Ω (above ~ 40 RPM). An increase in inertia properties tends to lower torque ripple at a given operating condition, but this may be costly. A reduction in gear ratio tends to lower apparent drive train rigidities and, thus, lower torque ripple. However, the most effective means of reducing torque ripple is through reduction of low speed rigidity. This can be shown as follows.

Let K_1 represent either the low speed (between the rotor and the transmission) drive train stiffness or the high speed (between the transmission and the generator) stiffness, and let K_2 represent the other. Assume that the high speed stiffness has been corrected to the low speed end by multiplying it by

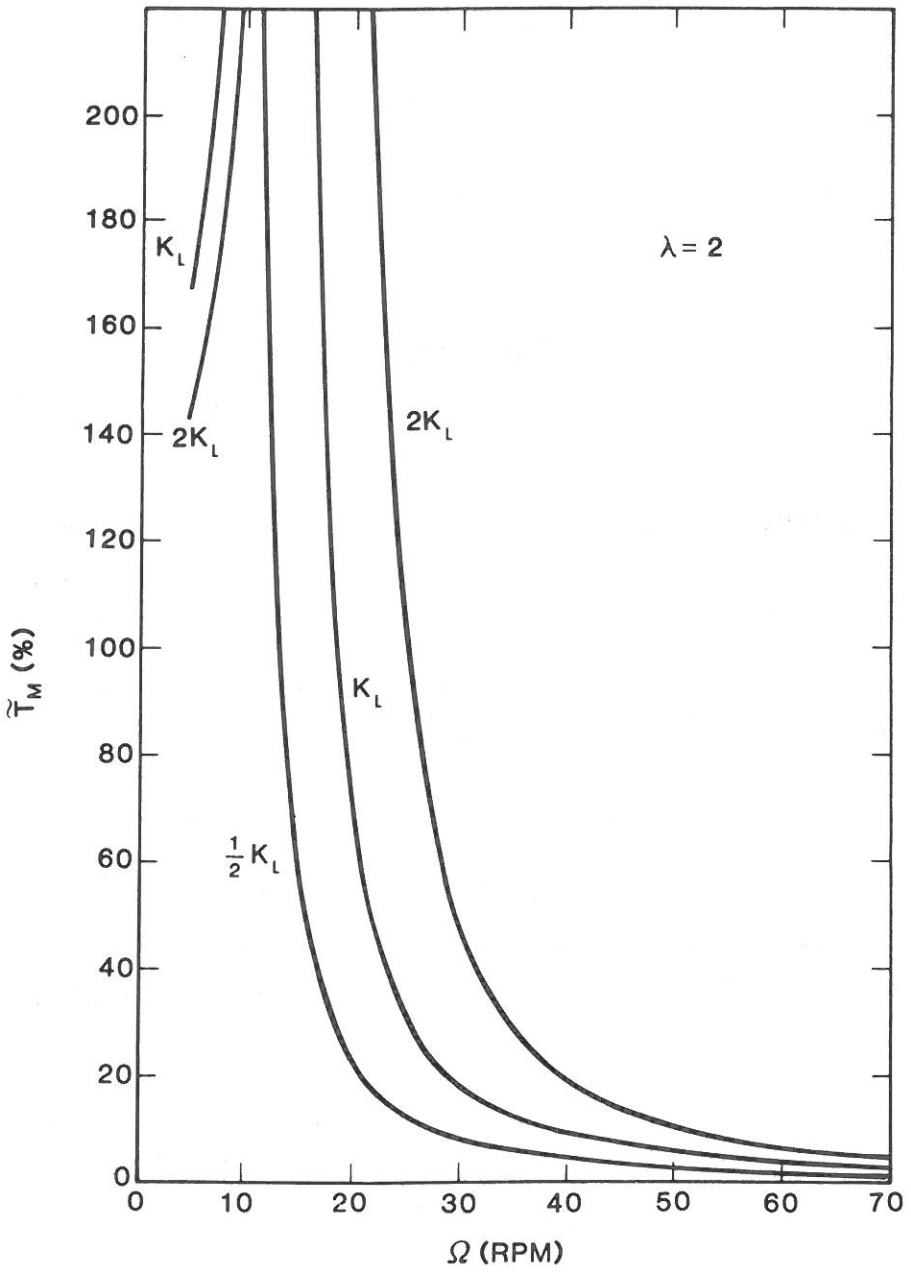

Figure 8. Torque ripple (expressed as a % of mean torque) versus turbine operating speed for various values of low speed drive train stiffness.

the square of the drive train speed ratio. Let the entire drive train stiffness by represented by $\overline{K}$. Then

$$\overline{K} = \frac{K_1 K_2}{K_1 + K_2} \tag{8}$$

The change in $\overline{K}$ can be expressed in terms of K_1 and K_2 and a change in either of these, say ΔK_1.

$$\frac{\Delta \overline{K}}{K} = \frac{\Delta K_1}{K_1} \left(\frac{K_2}{K_1 + K_2 + \Delta K_1} \right) \tag{9}$$

Now, let K_1 represent the high speed stiffness and recognize that $K_1 >> K_2$. From (9)

$$\lim \frac{\Delta \overline{K}}{K} \to 0 \text{ as } \frac{K_2}{K_1} \to 0$$

which implies that, for a given change in the high speed stiffness, the net effect is nearly zero. Now let K_2 represent the high speed stiffness and recognize that $K_2 >> K_1$. From (9)

$$\lim \frac{\Delta \overline{K}}{K} \to \frac{\Delta K_1}{K_1} \text{ as } \frac{K_1}{K_2} \to 0$$

This implies that a change in the new speed stiffness will result in approximately an equivalent change in the overall

drive train stiffness. Therefore, drive train stiffness changes are most effective when made at the low speed end. This result depends upon the high speed stiffness being much greater than the low speed stiffness, a condition which is nearly always true because of the effect that the speed ratio has on the high speed stiffness.

CONCLUSIONS AND RECOMMENDATIONS

Currently, the deterministic torque ripple problem is well understood. The source of torque ripple, its behavior with operating conditions, its response to property changes, and its allowable levels have been analytically predicted and experimentally verified. (Also, see Reference 1). Torque ripple in two-bladed VAWT systems can be maintained at acceptable levels.

As mentioned earlier, collection of data for correlation with the deterministic solution is difficult. This is due to the stochastic nature of the wind which tends to increase measured torque ripple in the turbine drive train above values predicted by the deterministic model. As turbines increase in size, their natural frequencies are reduced and their response times more nearly match the frequency content of the wind, thus aggravating the problem. Logically, the next step in torque ripple modeling should deal with the stochastic nature of the wind, in terms of both its magnitude and its direction. It is this author's feeling, however, that this additional characterization will have to begin with a modification of the aerodynamic codes which predict the torque applied to the turbine.

ACKNOWLEDGMENT

The willing and frequent assistance of G. M. McNerney, New Mexico Engineering Research Institute, University of New Mexico, in providing the Fourier coefficients of the applied torque used in the numerical evaluation of torque ripple is gratefully acknowledged.

REFERENCES

1. Reuter, R. C. and Worstell, M. H., "Torque Ripple in a Vertical Axis Wind Turbine," Sandia National Laboratories Report No. SAND78-0577, April 1978.

2. Mirandy, L. P., "Rotor/Generator Isolation for Wind Turbines," Journal of Energy, Vol. 1, No. 3, May-June, 1977.

3. Strickland, J. H., Webster, B. T., and Nguyen, T., "A Vortex Model of the Darrieus Turbine: An Analytical and Experimental Study," Sandia National Laboratories Report No. SAND79-7058, Feb. 1980.

4. Klimas, P. C., and Sheldahl, R. E., "Four Aerodynamic Prediction Schemes for Vertical Axis Wind Turbines: A Compendium," Sandia National Laboratories Report No. SAND78-0014, June 1978.

5. Worstell, M. H., "Aerodynamic Performance of the 17-Meter-Diameter Darrieus Wind Turbine," Sandia National Laboratories Report No. SAND78-1737, Jan. 1979.

6. McNerney, G. M., "Fourier Coefficients of Aerodynamic Torque Functions for the DOE/Sandia 17-M Vertical Axis Wind Turbine," Sandia National Laboratories Report No. SAND79-1508, Feb. 1980.

7. Lobitz, D. W. and Sullivan, W. N., "VAWTDYN--A Numerical Package for the Dynamic Analysis of Vertical Axis Wind Turbines," ASME Paper Presented at Nov. 1980 WAM.

8. Richards, C. W., Engineering Materials Science, Wadsworth Publishing Company, Inc., San Francisco, 1961.

9. Barton, R. S., Bowler, C. E. J. and Piwko, R. J., "Control and Stabilization of the DOE/NASA MOD-1 Two Megawatt Wind Turbine Generator," Proceedings, 14th Intersociety Energy Conversion Engineering Conference, Boston, MA, Aug, 1979.

DISTRIBUTION:

TID-4500-R66 UC-60 (283)

Aero Engineering Department (2)
Wichita State University
Wichita, KS 67208
Attn: M. Snyder
W. Wentz

R. E. Akins, Assistant Professor
Department of Engineering Science
and Mechanics
Virginia Polytechnic Institute and
State University
Blacksburg, VA 24060

Alcoa Laboratories (5)
Alcoa Technical Center
Aluminum Company of America
Alcoa Center, PA 15069
Attn: D. K. Ai
A. G. Craig
J. T. Huang
J. R. Jombock
P. N. Vosburgh

Mr. Robert B. Allen
General Manager
Dynergy Corporation
P.O. Box 428
1269 Union Avenue
Laconia, NH 03246

American Wind Energy Association
1609 Connecticut Avenue NW
Washington, DC 20009

E. E. Anderson
South Dakota School of Mines
and Technology
Department of Mechanical Engineering
Rapid City, SD 57701

Scott Anderson
318 Millis Hall
University of Vermont
Burlington, VT 05405

G. T. Ankrum
DOE/Office of Commercialization
20 Massachusetts Avenue NW
Mail Station 2221C
Washington, DC 20585

Holt Ashley
Stanford University
Department of Aeronautics and
Astronautics Mechanical Eng
Stanford, CA 94305

Kevin Austin
Consolidated Edison Company of
New York, Inc.
4 Irving Place
New York, NY 10003

F. K. Bechtel
Washington State University
Department of Electrical Eng
College of Engineering
Pullman, WA 99163

M. E. Beecher
Arizona State University
Solar Energy Collection
University Library
Tempe, AZ 85281

K. Bergey
University of Oklahoma
Aero Engineering Department
Norman, OK 73069

Steve Blake
Wind Energy Systems
Route 1, Box 93-A
Oskaloosa, KS 66066

Robert Brulle
McDonnell-Douglas Aircraft Corp
P.O. Box 516
Department 341, Building 32/2
St. Louis, MO 63166

R. Camerero
Faculty of Applied Science
University of Sherbrooke
Sherbrooke, Quebec
CANADA J1K 2R1

CERCEM
49 Rue du Commandant Rolland
93350 Le Bourget
FRANCE
Attn: G. Darrieus
J. Delassus

Professor V. A. L. Chasteau
School of Engineering
University of Auckland
Private Bag
Auckland, NEW ZEALAND

Howard T. Clark
McDonnell Aircraft Corporation
P.O. Box 516
Department 337, Building 32
St. Louis, MO 63166

Dr. R. N. Clark
USDA, Agricultural Research Serv
Southwest Great Plains Research
Bushland, TX 79012

Joan D. Cohen
Consumer Outreach Coordinator
State of New York
Executive Department
State Consumer Protection Board
99 Washington Avenue
Albany, NY 12210

Dr. D. E. Cromack
Associate Professor
Mechanical and Aerospace Eng
Department
University of Massachusetts
Amherst, MA 01003

Gale B. Curtis
Tumac Industries
650 Ford Street
Colorado Springs, CO 80915

DOE/ALO (3)
Albuquerque, NM 87185
Attn: G. P. Tennyson
D. C. Graves
D. W. King

DOE Headquarters (20)
Washington, DC 20545
Attn: L. V. Divone, Chief
Wind Systems Branch
D. F. Ancona, Program Mgr
Wind Systems Branch

C. W. Dodd
School of Engineering
Southern Illinois University
Carbondale, IL 62901

Dominion Aluminum Fabricating Ltd. (2)
3570 Hawkestone Road
Mississauga, Ontario
CANADA L5C 2U8
Attn: L. Schienbein
C. Wood

D. P. Dougan
Hamilton Standard
1730 NASA Boulevard
Room 207
Houston, TX 77058

J. B. Dragt
Nederlands Energy Research Found
Physics Department
Westerduinweg 3 Patten (nh)
THE NETHERLANDS

C. E. Elderkin
Battelle-Pacific Northwest Lab
P.O. Box 999
Richland, WA 99352

Frank R. Eldridge, Jr.
The Mitre Corporation
1820 Dolley Madison Blvd.
McLean, VA 22102

Electric Power Research Inst
3412 Hillview Avenue
Palo Alto, CA 94304
Attn: E. Demeo

James D. Fock, Jr.
Department of Aerospace Eng
University of Colorado
Boulder, CO 80309

Dr. Lawrence C. Frederick
Public Service Company of New Hamp
1000 Elm Street
Manchester, NH 03105

E. Gilmore
Amarillo College
Amarillo, TX 79100

Paul Gipe
Wind Power Digest
P.O. Box 539
Harrisburg PA 17108

Leander Nichols
Natural Power, Inc.
New Boston, NH 03070

Oklahoma State University (2)
Stillwater, OK 76074
Attn: W. L. Hughes
EE Department
D. K. McLaughlin
ME Department

Oregon State University (2)
Corvallis, OR 97331
Attn: R. E. Wilson
ME Department
R. W. Thresher
ME Department

Pat F. O'Rourke
Precinct 4
County Commissioner
City-County Building
El Paso, TX 79901

H. H. Paalman
Dow Chemical USA
Research Center
2800 Mitchell Drive
Walnut Creek, CA 94598

R. A. Parmelee
Northwestern University
Department of Civil Eng
Evanston, IL 60201

Helge Petersen
Riso National Laboratory
DK-4000 Roskilde
DENMARK

Wilson Prichett, III
National Rural Electric Coop
Association
1800 Massachusetts Avenue NW
Washington, DC 20036

Dr. Barry Rawlings, Chief
Division of Mechanical Eng
Commonwealth Scientific and Ind
Research Organization
Graham Road, Highett
Victoria, 3190
AUSTRALIA

Thomas W. Reddoch
Associate Professor
Department of Electrical Engineering
The University of Tennessee
Knoxville, TN 37916

A. Robb
Memorial University of Newfoundland
Faculty of Engineering and Applied Sci
St. John's Newfoundland
CANADA A1C 5S7

Dr.-Ing. Hans Ruscheweyh
Institut fur Leichtbau
Technische Hochschule Aachen
Wullnerstrasse 7
GERMANY

Gwen Schreiner
Librarian
National Atomic Museum
Albuquerque, NM 87185

Arnan Seginer
Professor of Aerodynamics
Technion-Israel Institute of
Technology
Department of Aeronautical
Engineering
Haifa, ISRAEL

Dr. Horst Selzer
Dipl.-Phys.
Wehrtechnik und Energieforschung
ERNO-Raumfahrttechnik GmbH
Hunefeldstr. 1-5
Postfach 10 59 09
2800 Bremen 1
GERMANY

H. Sevier
Rocket and Space Division
Bristol Aerospace Ltd.
P.O. Box 874
Winnipeg, Manitoba
CANADA R3C 2S4

P. N. Shankar
Aerodynamics Division
National Aeronautical Laboratory
Bangalore 560017
INDIA

David Sharpe
Kingston Polytechnic
Canbury Park Road
Kingston, Surrey
UNITED KINGDOM

D. G. Shepherd
Cornell University
Sibley School of Mechanical and
Aerospace Engineering
Ithaca, NY 14853

H. P. Sleeper
Kentin International
2000 Birdspring Road
Huntsville, AL 35802

Dr. Fred Smith
Mechanical Engineering Depart
Colorado State University
Ft. Collins, CO 80521

Kent Smith
Instituto Technologico Costa Rica
Apartado 159 Cartago
COSTA RICA

Leo H. Soderholm
Iowa State University
Agricultural Engineering
Ames, IA 50010

Southwest Research Institute (2)
P.O. Drawer 28501
San Antonio, TX 78284
Attn: W. L. Donaldson
R. K. Swanson

Rick Stevenson
Route 2
Box 85
Springfield, MO 65802

Dale T. Stjernholm, P.E.
Mechanical Design Engineer
Morey/Stjernholm and Associates
1050 Magnolia Street
Colorado Springs, CO 80907

G. W. Stricker
383 Van Gordon 30-559
Lakewood, CO 80228

C. J. Swet
Route 4
Box 358
Mt. Airy, MD 21771

R. J. Templin (3)
Low Speed Aerodynamics Section
NRC-National Aeronautical Establishment
Ottawa 7, Ontario
CANADA K1A OR6

Texas Tech University (3)
P.O. Box 4289
Lubbock, TX 79409
Attn: K. C. Mehta, CE Department
J. Strickland, ME Department
J. Lawrence, ME Department

Fred Thompson
Atari, Inc.
155 Moffett Park Drive
Sunnyvale, CA 94086

J. M. Turner, Group Leader
Terrestrial Energy Technology Program Off
Energy Conversion Branch
Aerospace Power Division
Aero Propulsion Laboratory
Department of the Air Force
Air Force Wright Aeronautical Laboratories
Wright-Patterson Air Force Base, OH 45433

United Engineers and Constructors, Inc.
Advanced Engineering Department
30 South 17th Street
Philadelphia, PA 19101
Attn: A. J. Karalis

University of New Mexico (2)
New Mexico Engineering Research Inst
Campus P.O. Box 25
Albuquerque, NM 87131
Attn: D. E. Calhoun
G. G. Leigh

University of New Mexico (2)
Albuquerque, NM 87106
Attn: K. T. Feldman
Energy Research Center
V. Sloglund
ME Department

Jan Vacek
Eolienne experimentale
C.P. 279, Cap-aux-Meules
Iles de la Madeleine, Quebec
CANADA

Irwin E. Vas
Solar Energy Research Inst
1617 Cole Blvd.
Golden, CO 80401

Otto de Vries
National Aerospace Lab
Anthony Fokkerweg 2
Amsterdam 1017
THE NETHERLANDS

R. Walters
West Virginia University
Department of Aero Eng
1062 Kountz Avenue
Morgantown, WV 26505

E. J. Warchol
Bonneville Power Admin
P.O. Box 3621
Portland, OR 97225

D. F. Warne, Manager
Energy and Power Systems
ERA Ltd.
Cleeve Rd.
Leatherhead
Surrey KT22 7SA
ENGLAND

R. A. Watson
Stanford University
546B Crothers Memorial Hall
Stanford, CA 94305

R. J. Watson
Watson Bowman Associates, Inc.
1280 Niagara St.
Buffalo, NY 14213

R. G. Watts
Tulane University
Department of Mechanical Eng
New Orleans, LA 70018

Pat Weis
Solar Energy Research Inst
1637 Cole Blvd.
Golden, CO 80401

W. G. Wells, P.E.
Associate Professor
Mechanical Engineering Depart
Mississippi State University
Mississippi State, MS 39762

T. Wentink, Jr.
University of Alaska
Geophysical Institute
Fairbanks, AK 99701

West Texas State University
Government Depository Library
Number 613
Canyon, TX 79015

Wind Energy Report
Box 14
104 S. Village Ave.
Rockville Centre, NY 11571
Attn: Farrell Smith Seiler

Richard E. Wong
Assistant Director
Central Solar Energy Research
Corporation
1200 Sixth Street
328 Executive Plaza
Detroit, MI 48226

1000 G. A. Fowler
1200 L. D. Smith
3141 T. L. Werner (5)
3151 W. L. Garner (3)
For DOE/TIC (Unlimited Rel)
3161 J. E. Mitchell (15)
3161 P. S. Wilson
4533 J. W. Reed
4700 J. H. Scott
4710 G. E. Brandvold
4715 R. H. Braasch (100)
4715 J. D. Cyrus
4715 R. D. Grover
4715 E. G. Kadlec
4715 P. C. Klimas
4715 M. T. Mattison
4715 R. O. Nellums
4715 W. N. Sullivan
4715 M. H. Worstell

5500 O. E. Jones
5510 D. B. Hayes
5520 T. B. Lane
5523 R. C. Reuter, Jr. (15)
5523 D. B. Clauss
5523 T. G. Carne
5523 J. R. Koteras
5523 D. W. Lobitz
5523 D. A. Popelka
5523 P. S. Veers
5530 W. Herrmann
5600 D. B. Schuster
5620 M. M. Newsom
5630 R. C. Maydew
5632 C. W. Peterson
5633 S. McAlees, Jr.
5633 R. E. Sheldahl
8266 E. A. Aas
DOE/TIC (25)
(R. P. Campbell, 3172-3)